Applied Surface Science 593 (2022) 153442

Contents lists available at ScienceDirect

Applied Surface Science

journal homepage: www.elsevier.com/locate/apsusc

Full Length Article

XPS spectra curve fittings of $Ti_3C_2T_x$ based on first principles thinking

Lars-Åke Näslund *, Ingemar Persson

Thin Film Physics Division, Department of Physics, Chemistry, and Biology (IFM), Linköping University, SE-581 83 Linköping, Sweden

ARTICLE INFO

Keywords:
MXene
2D materials
X-ray photoelectron spectroscopy
Peak fitting

ABSTRACT

MXenes are an interesting family of 2D materials that have the potential to meet challenges in many applications. A useful tool in the work of understanding the nature of the MXenes, as well as exploring their capabilities, is X-ray photoelectron spectroscopy (XPS). In analyzing XPS spectra it might be necessary to use curve fitting to extract valuable information. However, approaches toward the curve fitting procedure have been different in many studies and introductions of questionable assumptions, unverified feature assignments, and inconsistent curve fitting have led to contrasting conclusions from XPS analysis. It is therefore motivated to show curve fittings of F 1s, O 1s, Ti 2p, and C 1s XPS spectra obtained from high quality $Ti_3C_2T_x$ that are based on fundamental knowledge applied step by step through the strategy of first principles thinking. With the use of first principles thinking the curve fittings and the subsequent analysis became more realistic compared to what have been presented in recent studies. The results of the curve fittings presented in this work are well founded and can be used as a model for future curve fittings of MXenes. The strategy of first principles thinking is advantageous in XPS curve fittings in general.

1. Introduction

The new family of 2D-materials known as MXenes have shown great promise in a host of applications, such as supercapacitors [1], Li-ion batteries [2], fuel- and solar cells [3], transparent conductive electrodes [4], and composite materials with high strength [5]. The reason for the wide range of appealing technological use of MXenes is the large hydrophilic surface area conjoined with the high conductivity in the basal plane of the 2D-material. In addition, MXenes offer many different combinations of a transition metal (M), carbon or nitrogen (X), numerical proportions of atoms (n), and termination species (T_x) forming the $M_{n+1}X_nT_x$ compound that can be tailored for a specific application with fine-tuned properties [6,7]. The $M_{n+1}X_nT_x$ consists of n + 1 M-monolayers and n X-monolayers stacked in an alternated sequence where the first and the last M-monolayers form surfaces terminated by T_x. Until today there are about 30 different MXene compounds reported [8].

Preparing MXenes are comparatively easy, mainly because of their innate hydrophilicity. They can be synthesized by exfoliation of the parent precursor compounds MAX phases [9], which are nanolaminated phases of carbides and/or nitrides following the general formula $M_{n+1}AX_n$ (n = 1, 2, or 3) where A is a group A element in the Periodic Table [10]. To produce MXene the MAX phase is immersed in an acidic solution resulting in selective etching of the weakly bonded A-layers [11–13]. The termination species that inherently cover the surfaces of the formed 2D $M_{n+1}X_n$ layers depends on the selected etchant [14–16].

That MXenes have shown great promise in a variety of applications, not the least in energy storage [6,7], have made MXenes very popular. Among them is $Ti_3C_2T_x$ the most studied MXene. Even so, there is a need to increase our understanding of the interaction between the $M_{n+1}X_nT_x$ and its surrounding in a particular application. Because with an expanded knowledge, it might be possible to predict and improve the properties of MXenes. One popular tool for material characterization is X-ray photoelectron spectroscopy (XPS), which provides element-specific information on the electronic structures of the examined components. Through XPS it is possible to gain information about the chemical environment around the probed element, including the nature of the bonding to the nearest neighbor atoms. XPS analysis is, however, not always a simple task, especially if the material system contains unknown components and bonding configurations. XPS analysis on MXenes has shown to be challenging and until today there has not been a consensus regarding assignments of XPS features that appear in, e.g., XPS spectra of $Ti_3C_2T_x$ [17]. Deeper analysis of $Ti_3C_2T_x$ XPS data has been performed [13,17–21], but unfortunately, since the approaches have been different, the studies have reached different conclusions. Recently a review summarized the contrasting conclusions and made a

* Corresponding author.
E-mail address: lars-ake.naslund@liu.se (L.-Å. Näslund).

https://doi.org/10.1016/j.apsusc.2022.153442
Received 6 February 2022; Received in revised form 7 April 2022; Accepted 16 April 2022
Available online 19 April 2022
0169-4332/© 2022 The Authors. Published by Elsevier B.V. This is an open access article under the CC BY license (http://creativecommons.org/licenses/by/4.0/).

new attempt to critically analyze the XPS spectra of $Ti_3C_2T_x$ [17]. However, as new questionable assumptions, unverified feature assignments, and an inconsistent peak fitting method were introduced, the issue with contrasting conclusions from XPS analysis remains.

In this work, we will approach the XPS analysis with first principles thinking, which requires breaking down the analysis into fundamental steps where facts are separated from assumptions and then proceed with the analysis from the ground up. A prerequisite for successful XPS spectra analysis is, in most cases, a solid ground established from years of XPS investigations [22,23]. However, through first principles thinking, also known as first principles reasoning, we will use small pieces of knowledge that are self-evidently true and use those fundamental certainties in the curve fitting process. Hence, the reasoning from first principles thinking will lead to an XPS analysis that is more realistic than what has been presented in some of the recent studies [17,18,20,21].

In addition, the method of first principles thinking presented in this work is not limited to curve fittings of XPS spectra of $Ti_3C_2T_x$. On the contrary, the use of first principles thinking for reasonable XPS spectra curve fittings is an approach that can and should be applied every time XPS spectra are analyzed regardless of the material being investigated.

2. Methods

The XPS spectra presented in this work are obtained from two types of $Ti_3C_2T_x$ samples: freestanding $Ti_3C_2T_x$ film and thin film $Ti_3C_2T_x$ on sapphire substrate. The preparations of both the freestanding $Ti_3C_2T_x$ film and the thin film $Ti_3C_2T_x$ on sapphire substrate are presented in previous works [13,19,24,25]. The Ti_3AlC_2, and TiC samples were both thin films on sapphire substrates prepared through direct current magnetron sputtering of elemental Ti, Al, and C targets. The preparations of the Ti_3AlC_2, and TiC samples are presented in a previous work [13]. The commercially pure Al metal and the commercially pure Ti metal were obtained from Gränges Sweden AB and Permascand AB, respectively. Aluminum oxide (Al_2O_3) powder (ultra dry) was obtained from Sigma-Aldrich.

The XPS measurements were performed using the AXIS Ultra^{DLD} system from Kratos Analytical Ltd. with monochromatic Al Kα radiation and a pass energy (E_{pass}) of 20 eV. Further details are presented elsewhere [13,19].

The binding energy scale of all XPS spectra, presented herein, was carefully calibrated against the Fermi-edge (E_f), which was set to a binding energy of 0.00 ± 0.02 eV. The overall energy resolution obtained for the XPS spectra presented in this report was better than 0.3 eV, as determined through differentiation of the intensity over the Fermi edge. Normalization of all XPS spectra was performed at the background on the low binding energy side of the main peak/peaks. No Ar^+ sputtering was performed prior to XPS acquisition of the $Ti_3C_2T_x$, Ti_3AlC_2, TiC, and Al_2O_3 samples. The protective oxide layers on the commercially pure Al and Ti metal samples were, on the other hand, removed through Ar^+ sputtering for 3 min.

The curve fittings of the F 1s, O 1s, Ti 2p, and C 1s XPS spectra were performed using Igor Pro version 6.22A from WaveMetrics, which is a technical graphing and data analysis software for scientists and engineers [26].

3. Results and discussion

The most studied MXene so far is $Ti_3C_2T_x$ obtained from immersion of Ti_3AlC_2 powders in acidic solutions, such as 10–50% concentrated HF (aq) or a mixture of HCl(aq) and LiF(aq). The exfoliated Ti_3C_2-layers, about 0.5–2 μm large in diameter [1], have surfaces that are covered by termination species and adsorbates. It is important to distinguish between termination species and adsorbates, because termination species are essential for the formation of the delaminated Ti_3C_2-layers. The termination species have a similar function as the Al-layer in Ti_3AlC_2, i.e., to establish a redistribution of the delocalized electrons in the Ti_3C_2-layers that leads to a strengthening of the covalent Ti-C bonds [13]. Adsorbates, on the other hand, are atoms and molecules that exist on the $Ti_3C_2T_x$ surfaces in equilibrium with the surrounding at specific conditions. This distinction is also the reason why the termination species are very stable and difficult to remove or replace [16] while adsorbates exist on the surface only when the conditions are right. Examples of adsorbates are water (H_2O), hydrocarbons (CH_x), alcohols (C-OH), and nitrate/nitrite (NO_x). In addition, there might be impurities such as TiO_2, Al_2O_3, and graphite-like carbon in a $Ti_3C_2T_x$ sample [13].

3.1. Freestanding $Ti_3C_2T_x$ film versus thin film $Ti_3C_2T_x$ on sapphire substrate

The quality of a MXene sample depends very much on the quality of the original MAX phase, because the MXene can inherit impurities from the MAX-phase. For example, a freestanding $Ti_3C_2T_x$ film obtained from Ti_3AlC_2 powders prepared in an alumina tube furnace is incorporated with small amounts of non-reacted TiC, oxidized components (TiO_2 and Al_2O_3), and components from other side reactions. The fabrication of the freestanding $Ti_3C_2T_x$ film, which is a multi-step process that includes wet etching, cycles of washing, de-aerating, sonication, centrifugation, and filtering [24,25], might reduce the amount of impurities from the Ti_3AlC_2 powders preparation but at the same time introduce new impurities in one or several of the $Ti_3C_2T_x$ processing steps, such as metal halides, alcohols, and graphite-like materials (Figs. 1 and 2). Nevertheless, a well-prepared freestanding $Ti_3C_2T_x$ film can be of good quality [24,25]. Yet, it will not be as good as the quality of the thin film $Ti_3C_2T_x$ obtained from Ti_3AlC_2 prepared through direct current magnetron sputtering of elemental Ti, Al, and C targets in an ultrahigh-vacuum (UHV) system [13]. Not only that the controlled environment in the deposition system assures impurity-free Ti_3AlC_2 MAX-phase (although surface oxidation might occur when the sample is exposed to the atmosphere [13]), the Al removal to form $Ti_3C_2T_x$ requires only two steps: (1) immersion in 10% HF(aq) and (2) rinse in deionized water and ethanol.

The quality of a MXene sample might also depends on the storage condition before use. It is, for example, common that a batch of freestanding MXene film samples is produced at one occasion and stored until needed in a test, e.g. an electrochemical trial, or until available time slots for characterization. MXene samples in storage can degrade in many different processes, such as oxidation, disintegration, and contamination.

In the present work we will show XPS spectra from a freestanding $Ti_3C_2T_x$ film stored in protective N_2 atmosphere for six months (arbitrary selected storage length) with the aim to show that MXene samples might not always be of a quality good enough for trials, characterizations, and/or further investigations. Instead, a thin film $Ti_3C_2T_x$ on a sapphire substrate might be a preferably choice when accurate characterization and/or reliable investigation is on the agenda. This awareness is of course also needed when evaluating results or comparing results from different investigations.

3.2. Core-level XPS of freestanding $Ti_3C_2T_x$ film

Fig. 1 presents the F 1s, O 1s, Ti 2p, and C 1s XPS spectra of the freestanding $Ti_3C_2T_x$ film kept in protective N_2 atmosphere for six months. Through these four spectra we can evaluate the quality of the $Ti_3C_2T_x$ sample. The C 1s in Fig. 1(d) shows that graphite-like carbon, with a dominant peak at 285.3 eV, is mixed in with the $Ti_3C_2T_x$. In fact, the integrated intensity from the graphite-like carbon and adventitious carbon contamination is about 7 times larger compared with the corresponding integrated intensity of the carbide component at 282.0 eV. This finding is not unique for MXene samples, which raises the question if many of the studies presented in the literature actually are performed on graphite-like carbon with some minor MXene component. In addition

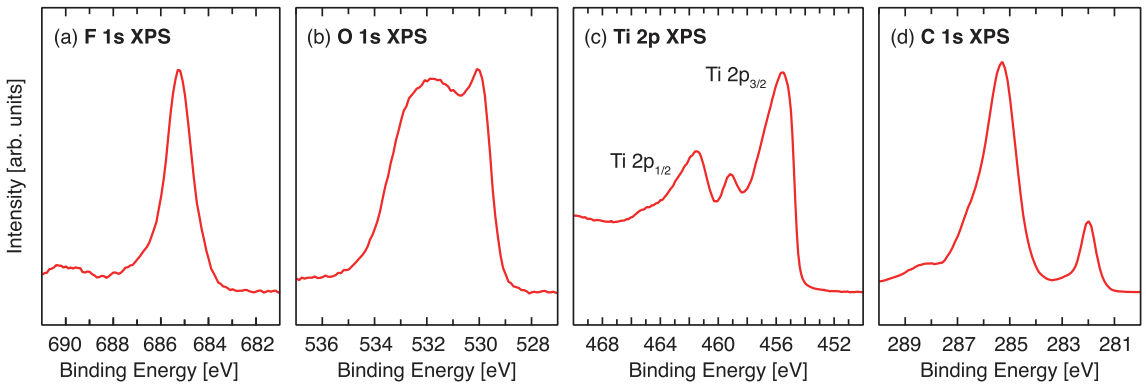

Fig. 1. XPS spectra of the freestanding $Ti_3C_2T_x$ film for the core levels (a) F 1s, (b) O 1s, (c) Ti 2p, and (d) C 1s. The photon energy was 1486.6 eV.

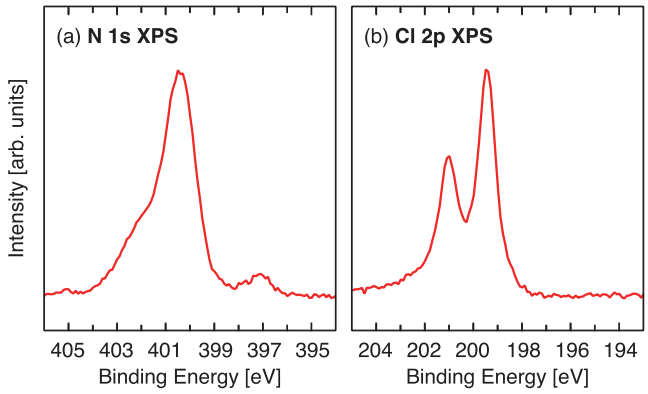

Fig. 2. XPS spectra of the freestanding $Ti_3C_2T_x$ film for the core levels (a) N 1s and (b) Cl 2p. The photon energy was 1486.6 eV.

there is a feature in the Ti 2p at 459.2 eV in Fig. 1(c) indicating oxidized sections of the $Ti_3C_2T_x$ surface. Also this finding raises the question if the active component in many $Ti_3C_2T_x$ studies actually is TiO_2 with O-vacancy sites, which is known to be functional for many processes [27–33]. Fig. 2 shows that nitrogen- and chlorine components also are present in the as-prepared sample. All nitrogen- and chlorine components are removed very easily through a moderate heating [25], which suggest that the nitrogen- and chlorine components are adsorbates.

The core-level XPS of the freestanding $Ti_3C_2T_x$ film shows that the sample, which is very easy to produce, has serious flaws. Results obtained from experiments using freestanding $M_{n+1}X_nT_x$ films should therefore be evaluated with care and healthy scientific skepticism. The core-level XPS spectra of the freestanding $Ti_3C_2T_x$ film presented in Fig. 1 can be curve fitted. However, separating the contributions from all the impurities and contaminations might require core-level XPS spectra from a $Ti_3C_2T_x$ reference sample that are free from non-MXene components, which will be presented next.

3.3. Core-level XPS of thin film $Ti_3C_2T_x$ on sapphire substrate

Fig. 3 presents the F 1s, O 1s, Ti 2p, and C 1s XPS spectra of the thin film $Ti_3C_2T_x$ sample. Fig. 3(d) shows a nice and sharp C 1s at 282.0 eV and comparatively very small amount of graphite-like carbon at 284.3 eV. The Ti 2p XPS spectrum in Fig. 3(c) shows no indication of TiO_2 formation, which otherwise would show a peak around 459 eV as shown in Fig. 1(c). The F 1s and O 1s spectra in Fig. 3(a) and (b), respectively, are strong and with clear details. Furthermore, nitrogen- and chlorine components, which were present in the freestanding $Ti_3C_2T_x$ film, are absent in the thin film $Ti_3C_2T_x$ sample. Hence, the quality of the $Ti_3C_2T_x$ sample is very good, which is a prerequisite for good studies in general and for XPS spectra curve fitting in particular. Hence, a thin film $Ti_3C_2T_x$ sample produced through HF(aq) etching of a well-defined thin film Ti_3AlC_2 MAX phase obtained from direct current magnetron sputtering of Ti, Al, and C targets in an ultra-high vacuum (UHV) environment [13,19] is pure enough for this work.

3.4. First principles thinking while curve fitting

Instead of immediate curve fitting of the XPS spectra we will use first principles thinking, which provides important details about the sample, the involved processes, and the spectra that we can break down into small pieces of knowledge. Hence, the curve fitting will then be based on facts of fundamental understanding and without any need of assumptions.

What we know about the photoelectric effect is that when a material is exposed to electromagnetic radiation there will be an emission of electrons given that the energy of the electromagnetic radiation is above

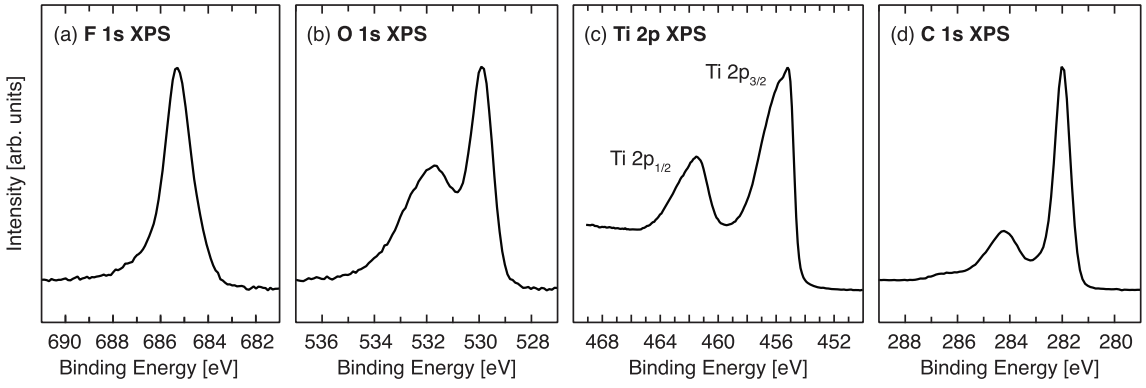

Fig. 3. XPS spectra of the thin film $Ti_3C_2T_x$ for the core levels (a) F 1s, (b) O 1s, (c) Ti 2p, and (d) C 1s. The photon energy was 1486.6 eV.

the binding energy of the emitted photoelectrons [34]. It is, thus, possible to determine the binding energy (E_B) of an electron in an orbital close to the nucleus of an element by simply subtracting the kinetic energy (E_k) of the emitted electron and the work function (φ) from the photon energy ($h\nu$) used to emit the electron, where φ is the energy needed to bring the electron from the sample surface into the electron energy analyzer [35]:

$$E_B = h\nu - (E_k + \varphi) \quad (1)$$

The obtained E_B for all escaping electrons depend on the element core level energies, i.e., from the orbitals close to the nucleus up to the valence band close to the Fermi level as shown in Fig. 4(a). The valence electrons have E_B in the range of 0–15 eV and at the Fermi-level the $E_B \equiv$ 0.0 eV, which appear as an edge (Fermi-edge) as shown in Fig. 4(b). If a recorded spectrum over the Fermi-edge shows that the Fermi-edge deviates from 0.0 eV the binding energy scale needs to be shifted for all core-level spectra. The shift required is the same value needed to bring the Fermi-edge to 0.0 eV. Fig. 4(b-c) demonstrates that the recorded spectrum over the Fermi-edge for the thin film $Ti_3C_2T_x$ on sapphire substrate shows that the binding energy scale must be shifted by −0.06 eV for all spectra obtained from the sample.

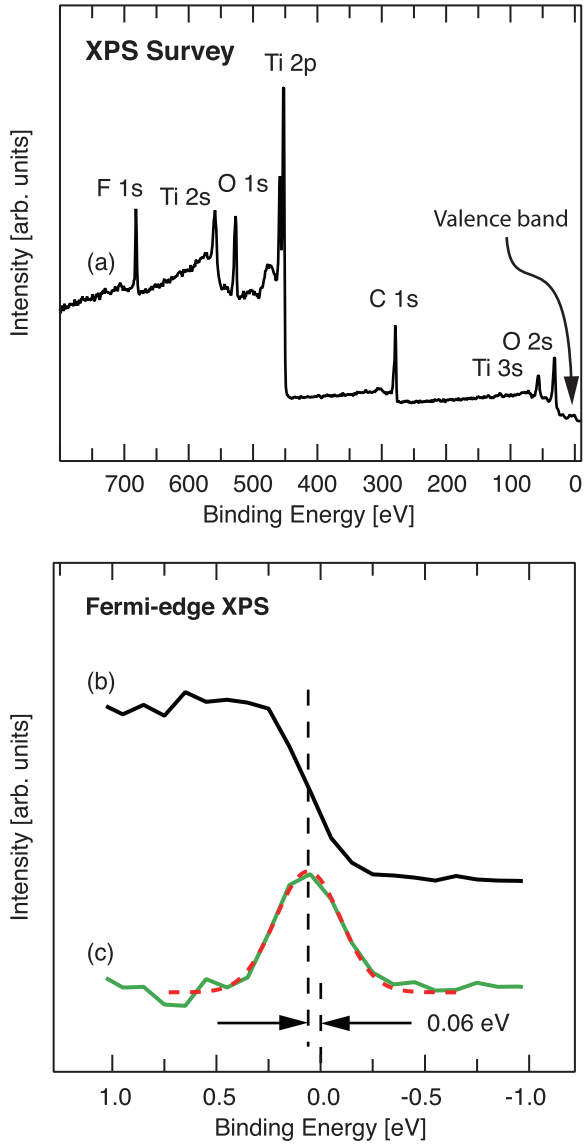

Fig. 4. (a) Survey XPS spectrum for $Ti_3C_2T_x$. (b) XPS spectrum over the Fermi-edge of the thin film $Ti_3C_2T_x$ on sapphire substrate. (c) The Fermi-edge position can easily be determined by differentiating the intensity over the edge (green solid line), which then is fitted by a Gaussian function (red dashed line). The deviation was determined to be 0.06 eV. The binding energy scale must therefore be shifted by −0.06 eV for all core-level spectra obtained from the thin film $Ti_3C_2T_x$ sample. The photon energy was 1486.6 eV. (For interpretation of the references to colour in this figure legend, the reader is referred to the web version of this article.)

All spectra presented in this work have their binding energy scale calibrated against the Fermi-edge. Unfortunately, there is a belief that the binding energy scale can be calibrated using the C 1s peak of adventitious carbon (hydrocarbon and graphite-like carbon). However, using the C 1s peak of adventitious carbon for binding energy scale calibration will lead to erroneous core-level binding energies [36] and should be avoided when samples have a clear Fermi-edge, i.e. all conducting samples. The main problem is that the adventitious carbon is a poor conductor and, thus, will shifts the C 1s peak of the hydrocarbon and graphite-like carbon when the C 1s electrons are consumed in the photoelectron process, i.e., charging of the adventitious carbon will shift the C 1s while the core-level XPS spectra of the conducting sample will not (when it is properly grounded). It is, for example, clear that the C 1s XPS peak of the hydrocarbon and graphite-like carbon has different positions for the freestanding $Ti_3C_2T_x$ film (285.3 eV) and the thin film $Ti_3C_2T_x$ on sapphire substrate (284.3 eV) while the carbide peak in both samples is located at 282.0 eV, as it should [17], because $Ti_3C_2T_x$ is a good conductor and the sample was properly grounded.

As shown in the survey XPS spectrum in Fig. 4(a), E_B depends on the core level energies of the elements in the sample. In addition is the E_B also sensitive to chemical bonding configurations. When the valence electrons of a probed element are involved in a chemical bonding they will be partly withdrawn from or attracted to the probed element, which will shift E_B toward higher or lower binding energy, respectively [35].

Hence, XPS can provide detailed information about the chemical environment around the probed element. However, for accurate interpretation it is necessary to be aware of the fundamental processes to which the photoelectrons from the probed core level energy may be exposed to and how it may affect the shape of the XPS spectrum.

For example, the O 1s XPS of Al_2O_3 presented in Fig. 5(a) shows that the detected photoelectrons have a binding energy distribution around the E_B, which mainly

depends on the core-hole lifetime and the instrumental imperfections [35]. The core-hole lifetime broadening and the instrumental broadening will distribute the photoelectron binding energy around E_B as a Lorentzian function and a Gaussian function, respectively. The convoluted Lorentzian and Gaussian functions are often called a Voigt function. Fig. 5(c) shows that the Voigt function, which is symmetric around E_B, fits the O 1s XPS spectrum of Al_2O_3 very well, although there is a small deviation around 532 eV. Adding a negative exponential function forming a tail on the Voigt function improves the curve fitting on the high binding energy side of E_B:

$$\text{Tail} = t_{amp}\exp(-(E - E_B)\, t_a), (E - E_B) > 0 \quad (2)$$

where t_{amp} is a pre-exponential constant for the tail height and t_a is a slope constant that determines how fast the tail is dampen. A tail on the high binding energy side is always present when there are free moving electrons in the material that interact with the photoelectron on its way out to the surface [35,37]. The interaction can be described as a convolution between a Bloch function and a Voigt function that generates harmonics, i.e. an intensity increase as a tail at the high binding energy side of E_B (0th harmonic) and satellites above E_B (n^{th} harmonics) evenly distributed with reducing intensities. A tail and satellites are, thus, always present in conducting materials, although the intensity of the satellites can be very small. Fig. 6(a, c).

shows the Al 2p and Ti 2p XPS of commercially pure Al and Ti metals, respectively, where Al 2p reveals strong intensity at the 1st and 2nd harmonics (the 3rd harmonic is superposed on the Al 2s peak) while the

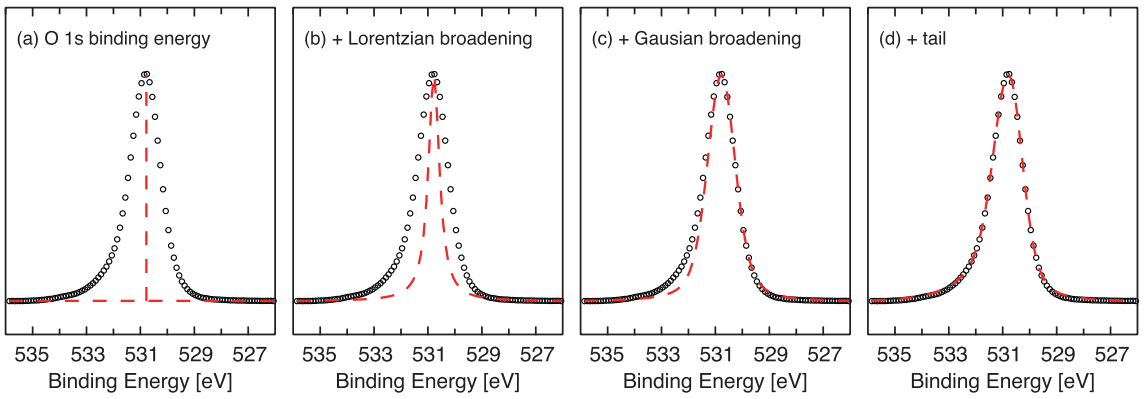

Fig. 5. O 1s XPS spectrum of Al_2O_3 where the curve fitting includes (a) only the E_B position, (b) the Lorentzian broadening added to E_B, (c) the Gaussian broadening convoluted to the Lorentzian broadening, and (d) a tail added to the Lorentzian-Gaussian function because some of the photoelectrons interacted with the low energy electrons that streamed to the probed volume from a flood gun. The photon energy was 1486.6 eV.

1st and 2nd harmonics from the Ti 2p show comparatively much lower intensities. The 0th harmonic, which appears as a tail on the main peaks, is more clearly shown in Fig. 6(b, d) where the tail is smaller for the Al 2p compared with the Ti 2p. Hence, the size of the tail depends on the conductivity but also on the intensity distribution over all harmonics. A perfect isolator, on the other hand, does not show any tail on the high binding energy side and the XPS peak is then symmetric on both sides of E_B. The O 1s XPS of Al_2O_3 in Fig. 5 should therefore show a symmetric peak, yet a tail was needed in the curve fitting as shown in Fig. 5(d). The reason is that an electron flood gun was supplying a stream of low energy electrons to compensate for the charging of the probed Al_2O_3, which otherwise would shift the XPS peak toward higher energies as the probed volume becomes depleted of electrons [38]. The stream of electrons will move toward the core-holes created in the photoemission processes and interact with some of the ejected photoelectrons resulting in a small tail.

According to first principles thinking it is necessary to break down our knowledge about XPS even further. That can be facilitated through simple questions, e.g., what can have influence on the full width at half maximum (fwhm) of the Voight function used in the curve fitting?

The core-hole lifetime broadening has to do with the interaction between the ejected photoelectron and the valence electrons that screen the atom core (nucleus + the core electrons + the core hole), which has to adjust to the new situation when the atom relaxes from the excited state by transferring an electron from a higher energy orbital down to the core hole accompanied by an ejection of an Auger-electron or fluorescence radiation [35]. If the time until relaxation (the core-hole lifetime) would be very much longer than the photoelectron emission process then the photoelectron would interact with a screening in balance (the coulomb balance between the valence electrons and the atom core). However, the time until relaxation is about the same as the duration of the photoelectron process and the photoelectrons from a large number of atoms in a sample will, with higher probability, interact with the atom core screening at different stages in the relaxation process and for different final states. Consequently, the distribution of the kinetic energy for the ejected photoelectrons becomes inversely proportional to the sum of all partial transition rates to various final states according to the Heisenberg uncertainty principle [39]. Hence, the fwhm of the Lorentzian (Γ) is inversely proportional to the core-hole lifetime (τ) through the reduced Planck constant (ħ):

$$\Gamma = \hbar\tau^{-1} \tag{3}$$

This is the reason why the $2p_{1/2}$ peak is in general broader than the $2p_{3/2}$ peak among transition metals. The lifetime of the $2p_{1/2}$ core hole is often shorter than the $2p_{3/2}$ core hole because of a possible Coster-Kronig decay channel where the core hole in the low energy $2p_{1/2}$ subshell is filled by an electron from a higher energy subshell of the same 2p orbital, which is a $2p_{3/2}$ electron [40]. In addition, valence electrons involved in chemical bonding may have some influence on the atom core screening, the relaxation process, and the interaction with the photoelectron, which can alter the core-hole lifetime [41]. For instance, the O 1s XPS of O, OH, and H_2O on Pt(1 1 1) shows that the core-hole lifetime broadening increases with the number of H bonded to the probed O [42].

The Gaussian broadening is assigned to instrumental imperfections, although there can be other contributions to the fwhm of the Gaussian part of the Voigt functions in the XPS spectrum curve fitting. One contribution is charging of the sample when a large number of core holes are created [43]. When core holes are created the probed sample becomes positively charged, which will shift the XPS peaks toward higher binding energies. If the created core holes in the probed volume are unevenly distributed, i.e. the different parts of the probed volume exhibits a spread in charge, then the kinetic energy of the emitted electrons will not be the same for all photoelectrons, which causes a Gaussian broadening around E_B. A perfectly grounded sample will not show this behavior, although most samples are not perfectly grounded locally around the probed volume. Another contribution to the fwhm of the Gaussian function is small variations in the neighborhood of the probed element, such as defects, different adsobates, and thermal vibrations, which will introduce slight adjustments in the chemical shifts of E_B [44]. The observed XPS feature will then be the sum of two or several XPS peaks with binding energies $E_B \pm \delta_i$, where δ_i is a significant shift of the binding energy for peak *i* that is too small to be perceptible except as a broadening of E_B. This can, for example, be reduced significantly by using perfectly cut and polished single crystal samples, perform the XPS in UHV, and using liquid N_2 cooling.

By breaking down our knowledge about XPS we have gathered many small pieces of information that will assist us when to curve fit the XPS spectra in Fig. 3. Let us use some of them when we curve fit the F 1s XPS spectrum in Fig. 3(a):

1. $Ti_3C_2T_x$ is conductive and the Voigt function must therefore be complemented with a tail.
2. An XPS peak with a tail is asymmetric around E_B in a way that the rising slope on the low binding energy side is steeper compared to the declining intensity on the high binding energy side as shown in Fig. 5 (d) and 6(d).

Piece of knowledge (PK) 1 tells us that a Voigt function with a tail is needed. However, the F 1s spectrum originates from termination species F on the $Ti_3C_2T_x$ surface and many photoelectrons can leave the surface without interaction with the free flowing electrons. The tail should therefore be comparatively small, which we also can see in Fig. 3(a). Although PK 2 tells us that the rising slope on the low binding energy

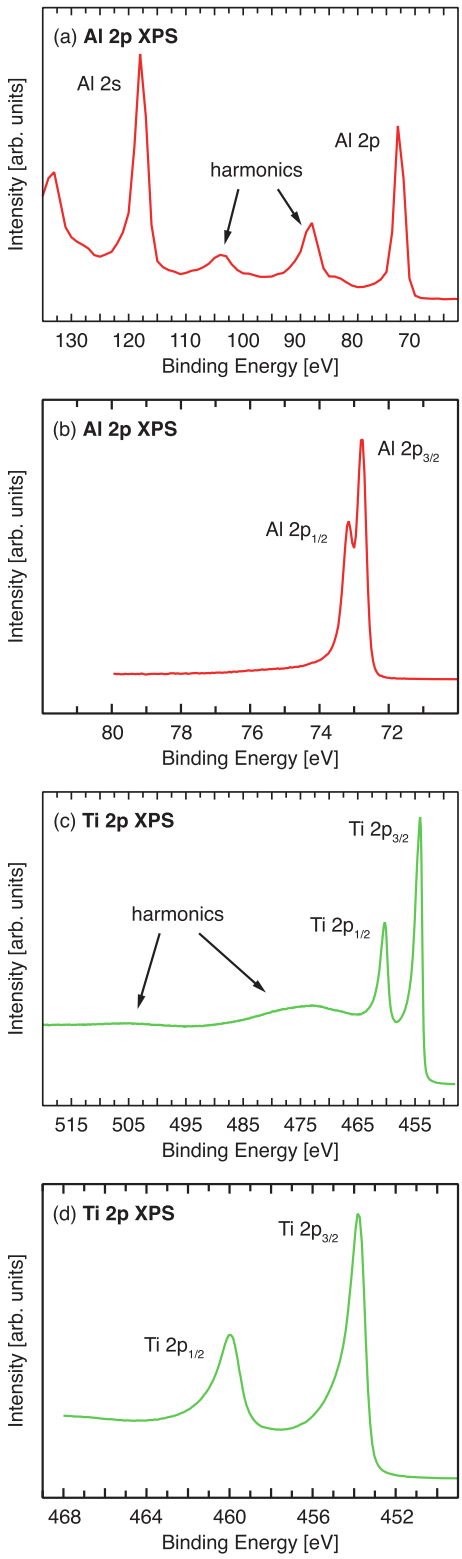

Fig. 6. XPS spectra of (a, b) commercially pure Al metal and (c, d) commercially pure Ti metal. Photoelectrons may interact with free moving electrons in the material, which results in a tail at the high binding energy side of E_B (0th harmonic), shown in (b) and (d), and satellites above E_B (n^{th} harmonics), shown in (a) and (c).

side normally is steeper compared to the declining intensity on the high binding energy side, the F 1s XPS of $Ti_3C_2T_x$ in Fig. 3(a) shows the opposite. That the rising slope on the low binding energy side appears to be less steep compared to the declining intensity on the high binding energy side is a clear indication of that the obtained XPS peak must consists of two features. Hence, the curve fitting must include two Voigt functions with tails. Fig. 7 presents the result from the curve fitting of the F 1s XPS spectrum of the thin film $Ti_3C_2T_x$. By using two identical Voigt functions with tails, except the amplitude, it is possible to achieve a very good fit when the Voigt functions are at 684.5 and 685.3 eV. It is clear that the component at 685.3 dominates and only about 20 % of the F atoms have an environment that shift E_B toward lower binding energies.

Next spectrum to curve fit is the O 1s XPS in Fig. 3(b). The shape of the O 1s XPS spectrum informs us that we need at least two components. PK 1 and 2 are valid also here and by examining the rising slope on the low binding energy side it was concluded that it should be possible to use one Voigt function with tail to fit the peak at 529.9 eV. The peak at 531.8 eV, on the other hand, overlaps with the peak at 529.9 eV and it is therefore impossible to see the rising slope on the low binding energy side of the peak. The peak at 531.8 eV is, in addition, broader compared to the peak at 529.9 eV and that raises the question if there is a need to use more than one Voigt function with tail to fit this feature? Using more than two Voigt functions with tails in the curve fitting of the O 1s XPS spectrum in Fig. 3(b) can only be motivated by a proven need, e.g., if there is a clear indication of the presence of more than two different oxygen containing termination species, adsorbates, and/or impurities. Can it, for example, be observed in the Ti 2p or C 1s XPS spectra that the sample has been oxidized or that a significant adsorption of organic molecules such as alcohols or carboxyl groups has occurred? It is, thus, necessary to take other core level XPS spectra of the sample and of

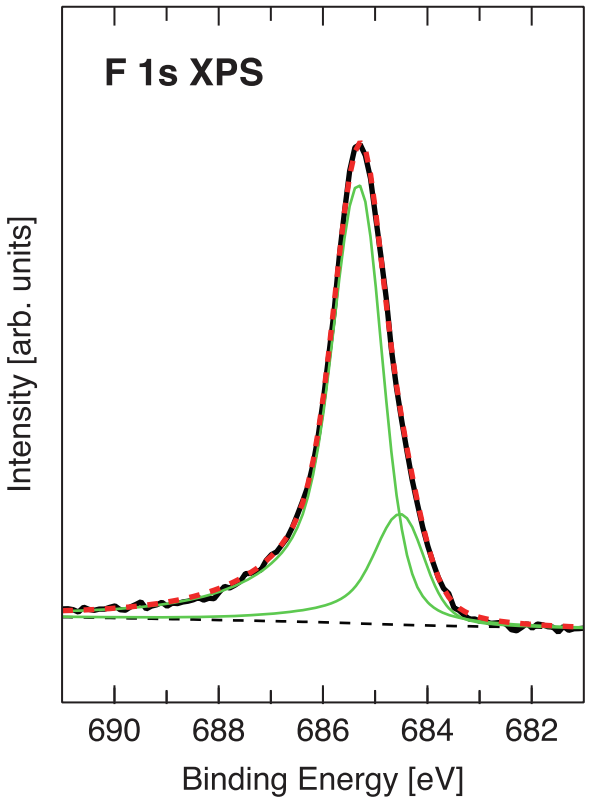

Fig. 7. The F 1s XPS of $Ti_3C_2T_x$ from Fig. 3(a). The spectrum is curve fitted using two Voigt functions with tails. The black and the red dashed lines are the Shirley background and the accumulated intensity of all fitted components, respectively. (For interpretation of the references to colour in this figure legend, the reader is referred to the web version of this article.)

related samples in consideration to gather important pieces of knowledge:

3. A Voigt function in a curve fitting of an XPS spectrum must be consistent with curve fittings of the other XPS spectra obtained from the sample.
4. A Voigt function in a curve fitting of an XPS spectrum must be consistent with curve fittings of corresponding XPS spectra obtained from related samples.

PK 3 means that it is necessary to consider possible O 1s components in the O 1s XPS spectrum in Fig. 3(b) by investigating, e.g., the Ti 2p and C 1s XPS spectra shown in Fig. 3(c-d). For example, a TiO_2 or a Ti_2O_3 (corundum) component must be present also in the O 1s XPS spectrum if there would be a TiO_2 component or a Ti_2O_3 component in the Ti 2p XPS spectrum. TiO_2 and Ti_2O_3 show a Ti $2p_{3/2}$ peak around 459 eV [33] and 458 eV [45], respectively, and a corresponding Ti $2p_{1/2}$ peak shifted 5.8 eV from the Ti $2p_{3/2}$ peak. There are, however, no indications of TiO_2 or Ti_2O_3 in the Ti 2p XPS spectrum shown in Fig. 3(c) and there is therefore no need to include a Voigt function representing a TiO_2 or Ti_2O_3 component in the O 1s XPS spectrum. The C 1s XPS spectrum in Fig. 3(d) shows, on the other hand, a small peak at 286.5 eV that probably originates from an alcohol component (C-OH), although, the amount is small enough to be disregarded in the O 1s XPS spectrum. Hence, the other XPS spectra from the sample, shown in Fig. 3, indicate that there is no need of a third Voigt function when to curve fit the O 1s XPS spectrum. However, PK 4 implies that it is not always enough to consider other XPS spectra from the sample. It may also be necessary to consider a corresponding XPS spectrum obtained from a related sample. In the case of O 1s XPS of $Ti_3C_2T_x$ it is, for example, relevant to consider the O 1s XPS of the Ti_3AlC_2 MAX phase, because there might be significant traces of residuals from the selective Al etching. It might be that oxygen-containing impurities in form of Al_2O_3 is present in the $Ti_3C_2T_x$ sample and therefore should be included in the curve fitting as a Voigt function with a tail at around 533 eV [13], although the contribution should be very small. Fig. 8 shows the Al 2p XPS of the thin film $Ti_3C_2T_x$, which confirms that a small amount of residual Al_2O_3 is present in the sample. Hence, a small contribution of Al_2O_3 must therefore be included in the curve fitting of the O 1s XPS spectrum.

In some of the previous curve fittings of the O 1s XPS spectrum of $Ti_3C_2T_x$ there have also been a Voigt function included that represents an OH component. However, a recent valence band UPS/XPS study showed that thin film $Ti_3C_2T_x$ on sapphire substrate and freestanding $Ti_3C_2T_x$ film (prepared from HF(aq) and a mixture of HCl(aq) and LiF (aq), respectively) do not inherently have OH as termination species [25].

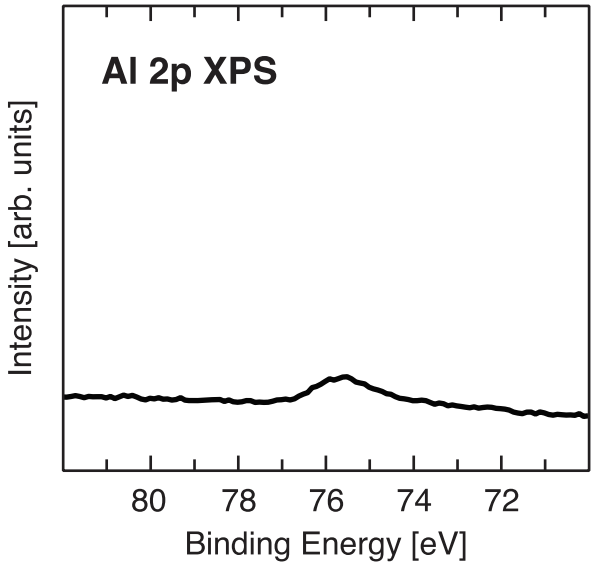

Fig. 8. The Al 2p XPS of the thin film $Ti_3C_2T_x$ on sapphire substrate. The feature at 75.6 eV indicates small amounts of residual Al_2O_3 in the sample.

Further, through first principles thinking we know that both the Lorentzian- and Gaussian-contributions in the Voigt function can have different fwhm:

5. The core-hole lifetime broadening becomes larger when the core–-hole lifetime becomes shorter.
6. The O 1s core-hole lifetime can become shorter when the number of bonds between the probed O and neighboring atoms increases.
7. Small variations in the environment of the probed O will induce small shifts in E_B that are too small to be perceptible except as a broadening of the O 1s XPS component.

To find out if PK 5–7 is valid we have to take into account corresponding XPS spectra obtained from a related sample in a previous study. A recent atomically resolved *in situ* scanning transmission electron microscopy (STEM) study, in combination with temperature-programmed XPS, came to the conclusion that a peak at 531.4 eV in the O 1s XPS of $Ti_3C_2T_x$ with only O as termination species originates from O coordinated to the face centered cubic (fcc) site, which is a hollow site formed by three surface Ti atoms in a triangular formation above a Ti atom in the inner Ti-monolayer [19]. The study further showed that when F also is present as a termination species the O occupation on the fcc-site is in competition with F and that the latter has precedence. Furthermore, with F in the neighborhood the O 1s XPS peak of O on the fcc-site is 531.8 eV but shifts to 531.4 eV when F is removed [19]. In addition, a recent valence band UPS/XPS study found that the alternative site for O is a bridge site between two surface Ti atoms [25]. Combining PK 5–7 with the observations in the temperature-programmed XPS/STEM study and the valence band UPS/XPS study leads to the insight that the O 1s XPS feature at 531.8 eV very well can be significantly broader compared to the feature at 529.9 eV. The reason is mainly because the E_B of the O termination species on the fcc-site is very much sensitive toward F in the neighborhood. An additional reason is that the O termination species on the fcc-site bonds to three Ti atoms, which can widen the core-hole lifetime broadening significantly compared to the O termination species on the bridge site that bonds to two Ti atoms [19,25,42].

Hence, according to first principles thinking it could very well be that the curve fitting of the O 1s XPS spectrum of $Ti_3C_2T_x$ only needs to include two Voigt functions with tails – one O species coordinated on the fcc-site and another on the bridge site. It is also reasonable, according to PK 5–7, that the O on the fcc-site may have an O 1s XPS peak with a significant wider fwhm compared to the O on the bridge site. One reason is because of a larger core-hole lifetime broadening originated from the increased number of bonding coordinations to the surface compared to the O on the bridge site. Another reason is the different possibilities of F in the close environment of the O on the fcc-site, which provides a small spread in E_B of the O 1s and thus a larger Gaussian broadening of the O 1s XPS peak. In addition to the O termination species there might also be a Voigt function with tail that corresponds to residual Al_2O_3 around 533 eV [13]. A Voigt function for an OH component is, on the other hand, not included in the curve fitting, which is based on the conclusion from the valence band UPS/XPS study [25]. Fig. 9 presents the result from the curve fitting of the O 1s XPS spectrum of the thin film $Ti_3C_2T_x$. As demonstrated, it is possible to achieve a very good fit by using two Voigt functions with tails that correspond to the termination species O occupying two different sites on the $Ti_3C_2T_x$ surfaces and one Voigt function with tail for residual Al_2O_3.

The third spectrum to curve fit is the C 1s XPS in Fig. 3(d). The peak shape at 282.0 eV in the C 1s XPS spectrum is typical for carbide materials [13]. In addition, there are features in the binding energy region 283–287 eV originating from graphite-like carbon [46], which is

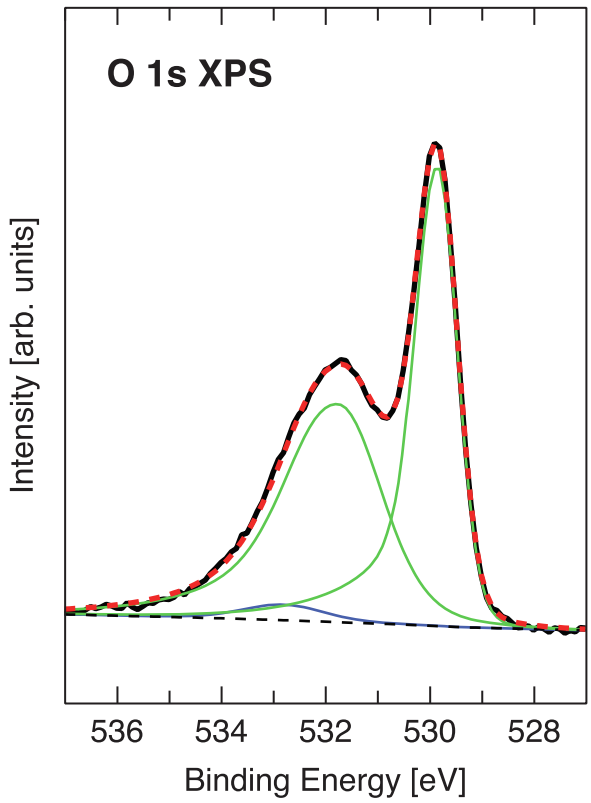

Fig. 9. The O 1s XPS of $Ti_3C_2T_x$ from Fig. 3(b). The spectrum is curve fitted using three Voigt functions with tails. The black and the red dashed lines are the Shirley background and the accumulated intensity of all fitted components, respectively. (For interpretation of the references to colour in this figure legend, the reader is referred to the web version of this article.)

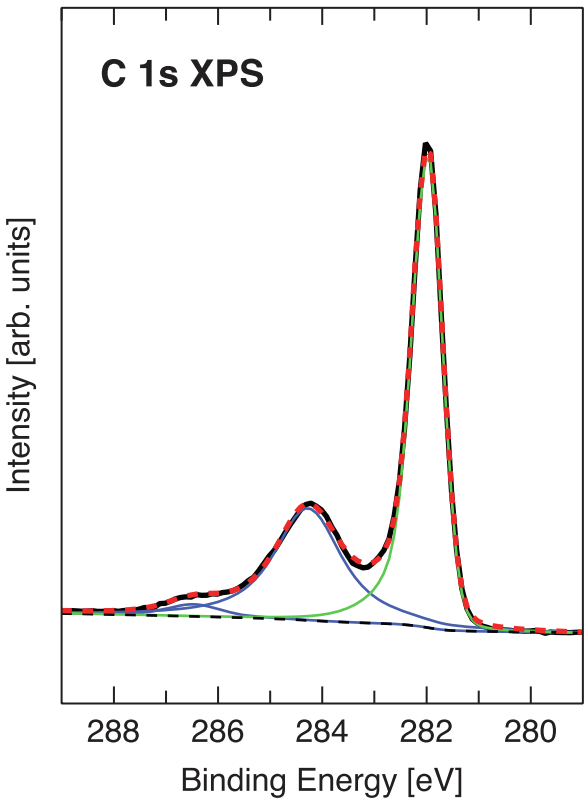

Fig. 10. The C 1s XPS of $Ti_3C_2T_x$ from Fig. 3(d). The spectrum is curve fitted using one Voigt functions with tail for the carbide peak at 282.0 eV and two symmetric Voigt functions for the graphite-like impurity and hydrocarbon and alcohol contamination. The black and the red dashed lines are the Shirley background and the accumulated intensity of all fitted components, respectively. (For interpretation of the references to colour in this figure legend, the reader is referred to the web version of this article.)

residual material from the etching of the Ti_3AlC_2 MAX phase, and contamination from the atmosphere in form of hydrocarbons and alcohols [47]. Since the carbide feature is clearly separated from the impurities and contaminations and the rising slope in the low binding energy side is steeper compared to the high binding energy side, we select to use one Voigt function with tail to fit the XPS peak at 282.0 eV (according to PK 1 and 2). The graphite-like carbon and the hydrocarbons are superposed into one feature at 284.3 eV while the alcohol feature is located at 286.5 eV. Because the graphite-like impurity and the hydrocarbon and alcohol contaminations are not a part of the conducting $Ti_3C_2T_x$ the two Voigt functions are symmetric, i.e., without tails. Fig. 10 presents the result from the curve fitting of the C 1s XPS spectrum of the thin film $Ti_3C_2T_x$.

The fourth and last spectrum to curve fit is the Ti 2p XPS in Fig. 3(c), which also is the most complicated spectrum to curve fit. The spin orbit split provides two XPS peaks where the intensity distribution is 2:1 between the $2p_{3/2}$ and $2p_{1/2}$ peaks [35]. Fig. 3(c) shows that the split between the $2p_{3/2}$ and $2p_{1/2}$ components is about 6 eV, which makes the curve fitting a little bit easier. A closer look at the Ti $2p_{3/2}$ reveals a shoulder on the high binding energy side, but except for the shoulder the Ti 2p XPS spectrum does not show any other features beyond the main peaks.

The curve fitting of the Ti 2p XPS spectrum will require all PK 1–7 and it is necessary to curve fit the F 1s, O 1s, and C 1s XPS spectra before a successful attempt to curve fit the Ti 2p XPS spectrum is possible. An important piece of knowledge is obtained from a corresponding XPS spectrum of $Ti_3C_2T_x$ with only O as termination species ($Ti_3C_2O_x$). The temperature-programmed XPS/STEM study found that when almost all F was removed the Ti $2p_{3/2}$ showed one sharp feature with tail not too different from the Ti $2p_{3/2}$ XPS of Ti_3AlC_2 MAX phase [13,19]. A Voigt function with a tail similar as used in the curve fitting of $Ti_3C_2O_x$ is therefore used to fit the sharp peak at 455.1 eV and a corresponding Voigt function with tail is used for the Ti $2p_{1/2}$ component. The remaining intensity must originate from Ti atoms that bond to F, which must be fitted with at least two Voigt functions with tails. Out of consistency, two Voigt functions with tails are needed to fit the Ti-F components in the Ti $2p_{3/2}$ XPS spectrum, because two Voigt functions with tails were required to fit the F 1s XPS spectrum. In fact, Fig. 11 shows that the three Voigt functions with tails at 455.1, 455.9, and 456.9 eV for the Ti $2p_{3/2}$ and the corresponding Voigt functions with tails at 461.3, 462.3, and 463.3 eV for the Ti $2p_{1/2}$ fit the Ti 2p XPS spectrum in Fig. 3 (c) very well.

3.5. Results from the curve fitting of the XPS spectra

Fig. 12 shows the outcome from the curve fittings of F 1s, O 1s, Ti 2p, and C 1s XPS spectra of the thin film $Ti_3C_2T_x$ sample.

In Fig. 12(a) we can see that two Voigt functions with tails were needed to fit the F 1s XPS spectrum. Given that F only occupies the fcc-site [19,25], the need to use two Voigt functions indicates that the F atoms on the fcc-sites have two different environments. We know that F is co-adsorbed with O, yet it is plausible that domains of only F exist on the $Ti_3C_2T_x$ surface. In such domains the F atoms do not have to share bonding from the Ti atoms with O. The charge transfer from the Ti atoms will then go to only the F atoms, which leads to more negatively charged F atoms compared to the F atoms in the domains where F is co-adsorbed with O. A more negative charge transfer to the F would shift the XPS peak toward lower binding energy. Hence the peak at 684.5 eV

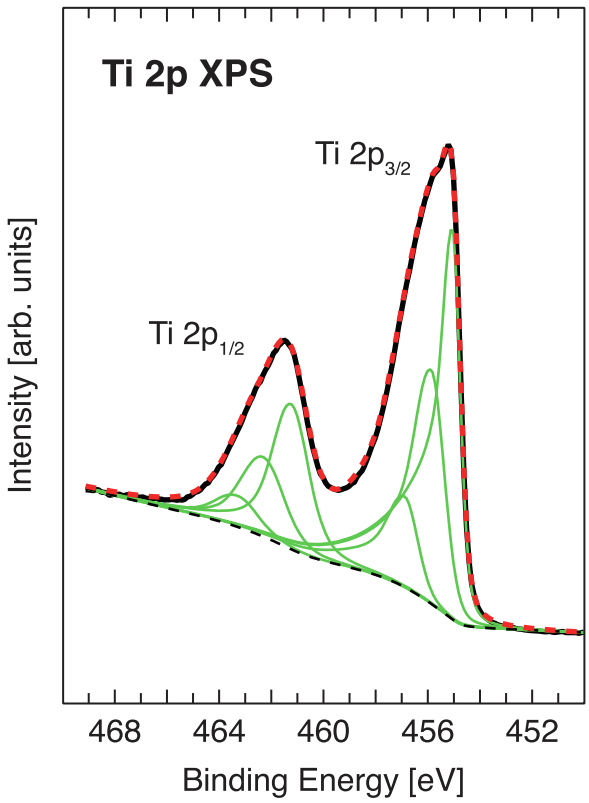

Fig. 11. The Ti 2p XPS of $Ti_3C_2T_x$ from Fig. 3(c). The spectrum is curve fitted using three Voigt functions with tails for the Ti $2p_{3/2}$ and corresponding Voigt functions for the Ti $2p_{1/2}$. The black and the red dashed lines are the Shirley background and the accumulated intensity of all fitted components, respectively. (For interpretation of the references to colour in this figure legend, the reader is referred to the web version of this article.)

originates from F in domains with only F atoms and the peak at 685.3 eV originates from F in domains where F is co-adsorbed with O. The intensity ratio between them is 1:5.

In Fig. 12(b) we can see that three Voigt functions with tails were needed to fit the O 1s XPS spectrum. The very small peak at 532.8 eV is associated with Al_2O_3 [13], a residual from the etching process of Ti_3AlC_2 MAX phase when making the $Ti_3C_2T_x$ MXene. The peaks at 529.9 and 531.8 eV originate, on the other hand, from the termination species O at two different sites. A previous work has identified the peak at 531.8 eV with O occupying the fcc-site [19] and a recent valence band UPS/XPS study has identified the peak at 529.9 with O occupying a bridge site between two surface Ti atoms [25]. The former peak is broader than the latter because of the increased core-hole lifetime broadening caused by the bonding toward three Ti atoms on the fcc-site compared to only two when O sits on the bridge site [42]. The different possibilities of F in the close environment of the O on the fcc-site will also increase the Gaussian broadening [19] compared to the O on the bridge site.

In Fig. 12(c) we can see that three pairs of Voigt functions with tails were needed to fit the Ti 2p XPS spectrum. The first pair of peaks, at 455.1 and 461.3 eV, has been attributed to Ti atoms bonded to O [19]. These peaks remain when all F atoms have been desorbed in a heating process leading to a $Ti_3C_2T_x$ surface covered only by O [19,25]. The second pair of peaks at 455.9 and 462.3 eV is assigned to Ti atoms bonded to both F and O in domains where F and O coexist. The third pair of peaks at 456.9 and 463.3 eV is, on the other hand, assigned to Ti atoms in the domains with only F. The second and third pairs of asymmetric Voigt functions used to fit the Ti 2p XPS spectrum correlate with the two peaks needed to fit the F 1s XPS spectrum in Fig. 12(a).

In Fig. 12(d) we can see that only one Voigt function with tail was needed to fit the carbide peak at 282.0 eV in the C 1s XPS spectrum. Two symmetric peaks were used to fit the graphite-like components + hydrocarbons at 284.3 eV and alcohol contaminations at 286.5 eV.

3.6. Discussions about the curve fitting of the XPS spectra

Fig. 12 shows that the accumulated intensity of all fitted components for each XPS spectrum follows the experimentally obtained spectrum perfectly for all four core-levels. That is also what a curve fitting process should aim for, although in combination with first principles thinking it can be difficult in some cases. Curve fittings of F 1s, O 1s, Ti 2p, and C 1s XPS spectra of $Ti_3C_2T_x$ MXene have been performed previously with various results [18–21]. The latest attempt was presented in Ref. [17], a work that also included a critical review of the previous curve fittings. The suggested curve fitting in Ref. [17] stands out particularly at one point – Tougaard functions were used as background representations.

Regarding background representation there are mainly three different background models used in curve fitting: linear, Shirley, and Tougaard [48]. A background representation using a linear function can be motivated when the difference in intensity before and after the XPS peak is small. It would, for example, be possible to use a linear background representation for the F 1s XPS spectrum in Fig. 3, because the intensity at 679–682 eV (before the F 1s XPS peak) and the intensity at 692–695 eV (after the F 1s XPS peak) are about the same. A linear background representation would also work for the O 1s spectrum and maybe even for the C 1s XPS spectrum. The Ti 2p XPS spectrum in Fig. 3

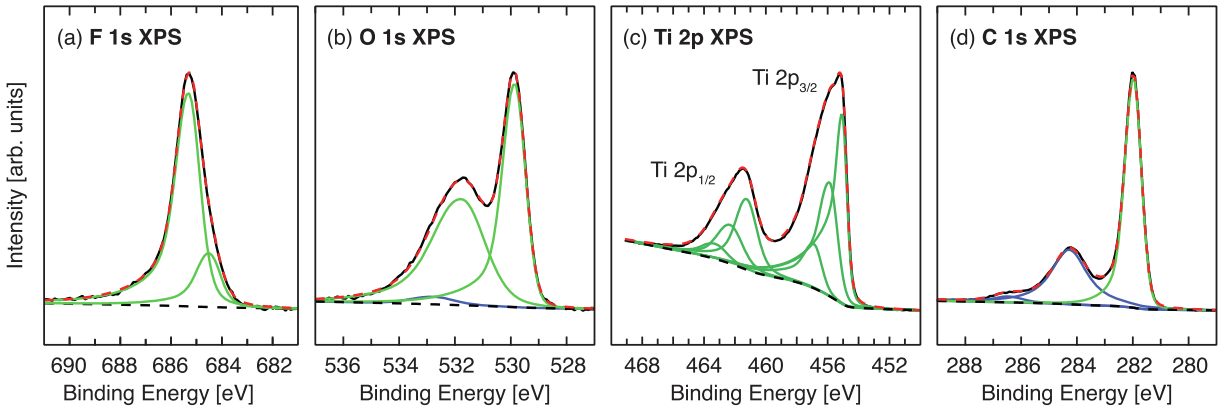

Fig. 12. Curve fittings of the XPS spectra for (a) F 1s, (b) O 1s, (c) Ti 2p, and (d) C 1s obtained from the thin film $Ti_3C_2T_x$. The black and the red dashed lines are the Shirley background and the accumulated intensity of all fitted components, respectively. The photon energy was 1486.6 eV. (For interpretation of the references to colour in this figure legend, the reader is referred to the web version of this article.)

(c), on the other hand, requires a better background model. The background is mainly derived by inelastic scattered photoelectrons, but also by secondary electrons and inelastic scattered Auger electrons [35]. The background contribution across the Ti 2p XPS spectrum is not perfectly modeled by either the Shirley function or the Tougaard function [48]. Nevertheless, the Shirley function and the Tougaard function are easy to apply and are very often included in XPS curve fitting software's. The one to use depends on the binding energy range in the recorded XPS spectrum [48]. The Tougaard function was developed for long-range background representation [49] and would be suitable for the Ti 2p XPS in Fig. 6(c) where the binding energy range is more than 50 eV. For a shorter binding energy range, e.g. the Ti 2p XPS in Fig. 6(d), the Tougaard function is less successful and very often causes an abrupt kink in the background representation where the Tougaard function meets the spectrum at the high binding energy side [48]. If a kink appears in the background subtracted XPS spectrum after using a Tougaard function, see for example Fig. 14(a) in Ref. [17], then an alternative background representation must be selected, because the kink is both arbitrary and physically unreasonable [48]. It is necessary to select a function for the background representation that merges smoothly with the recorded background on the high binding energy side of the main peaks. That is something the Shirley function can do and is therefore the preferable background representation for narrow binding energy ranges [50], such as the Ti 2p XPS spectrum in Fig. 3(c). Notably, in the curve fittings of all XPS spectra in Fig. 3 the backgrounds were represented by Shirley functions, as shown in Fig. 12.

It is also important to point out that if the curve fitting is a part of a quantification procedure, then the binding energy range for the Ti 2p XPS spectrum must be something like 70 eV. This is because the satellites around 475 and 505 eV (see Fig. 6(c)) should not be considered as part of the background. Especially not the former since it overlaps with the Ti 2p main peaks. In the present work, on the other hand, the aim of the curve fitting is to find the components that contribute to the Ti 2p XPS spectrum and what E_B they have. For that a Shirley function is sufficient as a background representation in the main Ti 2p XPS region at 450–469 eV.

One challenge in the curve fitting of the Ti 2p XPS spectrum of $Ti_3C_2T_x$ shown in Fig. 3(c) is to estimate the sizes of the tails on the asymmetric Voigt functions. However, by removing all F in a heat treatment it is possible to see the tail for the Ti 2p component at 455.1 eV [19]. Fig. 13 shows the Ti 2p XPS spectra for Ti metal, TiC, Ti_3AlC_2 MAX phase, and thin film $Ti_3C_2T_x$ where almost all F is removed through a heat treatment ($Ti_3C_2O_x$); curve fitting of each spectrum is presented in Ref. [13] for the Ti metal, TiC, and Ti_3AlC_2 MAX phase and in Ref. [19] for the thin film $Ti_3C_2O_x$. Fig. 13(d) shows that the Ti-O component at 455.1 eV in the thin film $Ti_3C_2T_x$ has a tail that is not far from the corresponding tail in Ti metal. In fact, the differences in shape between all four Ti $2p_{3/2}$, including the tails, are very small. The Ti metal in Fig. 13 (a) is commercially pure and does not have any other components than Ti metal in the Ti 2p XPS spectrum. Hence, the comparison in Fig. 13 shows that the selected tail to the Voigt function representing Ti-O component at 455.1 eV in Figs. 11 and 12(c) is the correct one to use, because it is based on the curve fitting of the thin film $Ti_3C_2T_x$ where almost all F is removed. The shape of the Ti-O component at 455.1 eV in the curve fitting performed in Ref. [17] is, on the other hand, not similar to either the Ti metal, TiC, or Ti_3AlC_2 MAX phase, which will negatively affect the whole curve fitting procedure.

The selection of a suitable background representation and the usage of an appropriate tail on the Voigt function representing the Ti-O component at 455.1 eV are essential for a proper curve fitting of the Ti 2p XPS spectrum of the thin film $Ti_3C_2T_x$. Failing with the background representation and with the tail on the Voigt function representing the Ti-O component at 455.1 eV may lead to deceiving peaks that have no support from first principles reasoning.

To complete the curve fitting of the Ti 2p XPS in Fig. 3(c) it was necessary to add only two Voigt functions with tails that represents the two Ti-F components we know must be included based on the curve fitting of the F 1s spectrum as shown in Fig. 7. With two identical Voigt functions with tails, except the amplitudes, the two Ti-F components could easily be fitted at 455.9 and 456.9 eV. It would be possible to add three identical Voigt functions with tails with reducing amplitudes, although there is no support from the first principles reasoning that three Voigt functions are needed. Each surface Ti atom is surrounded by three fcc-sites and, thus, there are ten possible combinations that F, O, and vacancy (–) can be distributed around a surface Ti atom. However,

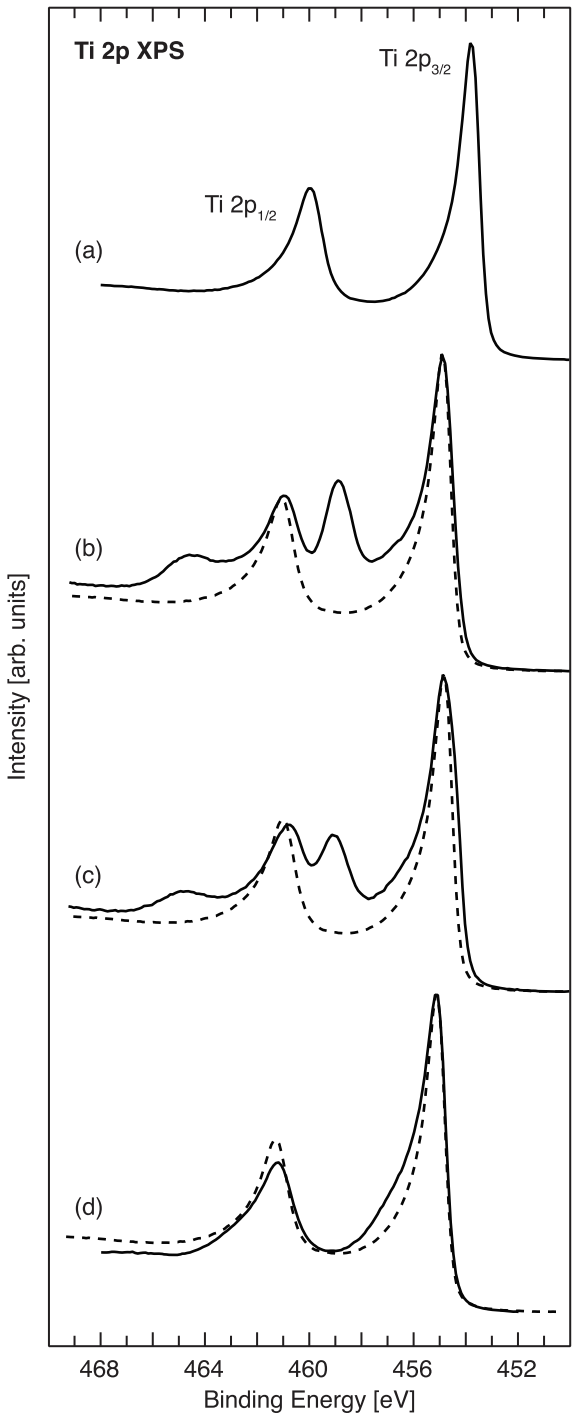

Fig. 13. Ti 2p XPS spectra of (a) Ti metal, (b) TiC, (c) Ti_3AlC_2 MAX phase, and (d) the thin film $Ti_3C_2T_x$ where almost all F is removed through a heat treatment. The dashed spectrum in (b), (c), and (d) is the Ti metal spectrum in (a) shifted to align with the Ti $2p_{3/2}$. The photon energy was 1486.6 eV.

the three dominating distributions are most likely F/F/F, F/O/–, and O/O/–, which is based on the observation of that it is about the same amount of F_{fcc}, O_{fcc}, and O_{bridge} in the $Ti_3C_2T_x$ sample used in this study and that all O_{bridge} is not transferred to all vacant fcc-sites when all F is removed from the $Ti_3C_2T_x$ surface [19]. However, as long as a closer study of the coverage of a well-defined $Ti_3C_2T_x$ surface is not completed, this is only mere speculation and does not coincide with first principles thinking. Hence, using three pairs of Voigt functions with tails in the curve fitting of the Ti 2p XPS spectrum in Fig. 3(c) are motivated by the first principles thinking and additional Voigt functions have to wait until more evidence that support additional Voigt functions are provided, if that would be the case.

A relevant question is whether there should also be two Ti-O components in the Ti 2p XPS spectrum, because there are two features in the O 1s XPS spectrum? The answer is: not necessarily. The peak at 529.9 eV originates from O in a bridge position between two surface Ti atoms [19,25] and all the O_{bridge} are moving around rapidly over the $Ti_3C_2T_x$ surface [51]. Hence, the contribution from the Ti-O_{bridge} is distributed over the Ti-O_{fcc} component and the two Ti-F_{fcc} components, because the Ti atoms that bond to the O on the bridge sites also bond to the O and F on the fcc-sites. This is clear in Fig. 13(d), which shows the Ti 2p XPS spectrum of $Ti_3C_2O_x$ where the O atoms are occupying both the fcc-sites and the bridge sites [19,25], where only one Ti $2p_{3/2}$ component is present, except a small feature around 457 eV showing that all F are not removed from the $Ti_3C_2T_x$ surface [19].

Regarding the O 1s XPS spectrum in Fig. 3(b) – are there reasons to include more than two Voigt functions with or without tails in the curve fitting of the O 1s XPS spectrum? Other possible contributions to the O 1s XPS spectrum of $Ti_3C_2T_x$ are different oxygen containing termination species, adsorbates, and impurities. Considering other oxygen containing termination species there have been numerous publications proposing the hydroxide (OH) as a termination species. There have been a few attempts to provide evidences for OH being a termination species [18,52], although the results have not been without doubts [19] as OH is a common adsorbate on the TiO_2 and Al_2O_3 impurities [27–33]. On the contrary, a recent valence band UPS/XPS study provided a clear evidence against OH as an inherently formed termination group on the $Ti_3C_2T_x$ surfaces [25]. Considering oxygen containing adsorbates and impurities there have been extra precautions to avoid significant amounts of adsorbates and impurities on the $Ti_3C_2T_x$ surface, which is evident from the absent TiO_2 feature in the Ti 2p XPS spectrum in Fig. 3(c) and the low amount of adventitious carbon in the C 1s XPS spectrum in Fig. 3(d). In addition, there are no shoulders or other features in the O 1s XPS spectrum in Fig. 3(b) that would motivate any additional Voigt functions in the curve fitting process. The only indication of any oxygen containing adsorbate and impurity is a very small amount of residual Al_2O_3, which has a component in the O 1s XPS spectrum at 532.8 eV. Furthermore, according to first principles thinking there is no evidence in the provided data in this work or in other related works [13,19,25] that motivates more components than those that are already included in the O 1s XPS spectrum presented in Figs. 9 and 12(b).

Hence, through first principles thinking we have arrived in seven pieces of knowledge important in the process of the curve fittings of the F 1s, O 1s, Ti 2p, and C 1s XPS spectra obtained from $Ti_3C_2T_x$ MXene:

1. $Ti_3C_2T_x$ is conductive and the Voigt function must therefore be complemented with a tail.
2. An XPS peak with a tail is asymmetric around E_B in a way that the rising slope on the low binding energy side is steeper compared to the declining intensity on the high binding energy side.
3. A Voigt function in a curve fitting of an XPS spectrum must be consistent with curve fittings of the other XPS spectra obtained from the sample.
4. A Voigt function in a curve fitting of an XPS spectrum must be consistent with curve fittings of corresponding XPS spectra obtained from related samples.
5. The core-hole lifetime broadening becomes larger when the core-hole lifetime becomes shorter.
6. The O 1s core-hole lifetime can become shorter when the number of bonds between the probed O and neighboring atoms increases.
7. Small variations in the environment of the probed O will induce small shifts in E_B that are too small to be perceptible except as a broadening of the O 1s XPS component.

These pieces of knowledge are established [35–44,48–50] and supported the curve fitting procedure significantly. Background representations that smoothly merged with the recorded intensities before and after the main peak/peaks in the XPS spectra and a thoroughly selected tail for the Voigt function representing the Ti-O component at 455.1 eV were also essential contributions. That the sample was of good quality and almost free from impurities, adsorbates, and contaminations paved the way for a curve fitting procedure without guessing or using assumptions, which is the basic idea of using first principles thinking.

Instead we could acquire information about the $Ti_3C_2T_x$ MXene from the results of the curve fittings. For example:

- Charge transfer occurs from the Ti atoms to the termination species F and O.
- The F atoms attract more charge from the Ti atoms compared to the O atoms.
- The O component at 529.9 eV bonds toward fewer Ti atoms compared to the O component at 531.8 eV, which supports the finding of that the former is O on the bridge site between two surface Ti atoms and the latter is O on the fcc-site formed by three surface Ti atoms [19,25].
- There are at least two domains on the $Ti_3C_2T_x$ surface where one domain, which corresponds to about 20 % of the $Ti_3C_2T_x$ surface, has only F on the fcc-sites while the other domain has both F and O on the fcc-sites.

4. Conclusions

Through first principles thinking it was possible to perform curve fittings of the F 1s, O 1s, Ti 2p, and C 1s XPS spectra from high quality $Ti_3C_2T_x$ MXene without using assumptions. Instead, a detailed understanding of the XPS spectra was deduced by guidance from seven pieces of well-established XPS knowledge. Information from other relevant reference samples gave essential details needed to proceed without the risk of introducing errors in the curve fittings. It was also important to select background representations that smoothly merged with the recorded intensities before and after the main peak/peaks in the XPS spectra. The obtained curve fittings are well founded and should be used as a model for future curve fittings of XPS spectra of MXene materials in particular, but also other conducting materials in general. Furthermore, well-performed curve fittings of high quality XPS spectra can provide more information about the sample of investigation than mere element identification and their oxidation states.

CRediT authorship contribution statement

Lars-Åke Näslund: Conceptualization, Methodology, Validation, Formal analysis, Investigation, Resources, Writing – original draft, Visualization. **Ingemar Persson:** Writing – review & editing, Supervision.

Declaration of Competing Interest

The authors declare that they have no known competing financial interests or personal relationships that could have appeared to influence the work reported in this paper.

Acknowledgements

The study has partly been accomplished through funding from the Swedish Foundation for Strategic Research (SSF) through program funding (EM16-0004), the Swedish Research Council (VR) grant no. 642-2013-8020, and the KAW Fellowship/Scholar program.

References

[1] M. Ghidiu, M.R. Lukatskaya, M.-Q. Zhao, Y. Gogotsi, M.W. Barsoum, Conductive Two-Dimensional Titanium Carbide 'Clay' with High Volumetric Capacitance, Nature 516 (2014) 78–U171.
[2] M. Naguib, J. Halim, J. Lu, K.M. Cook, L. Hultman, Y. Gogotsi, M.W. Barsoum, New Two-Dimensional Niobium and Vanadium Carbides as Promising Materials for Li-Ion Batteries, J. Am. Chem. Soc. 135 (43) (2013) 15966–15969.
[3] N. Li, X. Chen, W.-J. Ong, D.R. MacFarlane, X. Zaho, A.K. Cheetham, C. Sun, Understanding of Electrochemical Mechanisms for CO_2 Capture and Conversion into Hydrocarbon Fuels in Transition-Metal Carbides (MXenes), ACS Nano 11 (2017) 10825–10833.
[4] J. Halim, M.R. Lukatskaya, K.M. Cook, J. Lu, C.R. Smith, L.-Å. Näslund, S.J. May, L. Hultman, Y. Gogotsi, P. Eklund, M.W. Barsoum, Transparent Conductive Two-Dimensional Titanium Carbide Epitaxial Thin Films, Chem. Mater. 26 (7) (2014) 2374–2381.
[5] X. Li, X. Yin, C. Song, M. Han, H. Xu, W. Duan, L. Cheng, L. Zhang, Self-Assembly Core-Shell Graphene-Bridged Hollow MXenes Spheres 3D Foam with Ultrahigh Specific EM Absorption Performance, Adv. Funct. Mater. 28 (2018) 1803938.
[6] Y.u. Xie, Y. Dall'Agnese, M. Naguib, Y. Gogotsi, M.W. Barsoum, H.L. Zhuang, P.R. C. Kent, Prediction and Characterization of MXene Nanosheet Anodes for Non-Lithium-Ion Batteries, ACS Nano 8 (9) (2014) 9606–9615.
[7] M. Naguib, V.N. Mochalin, M.W. Barsoum, Y. Gogotsi, 25th Anniversary Article: MXenes: A New Family of Two-Dimensional Materials, Adv. Mater. 26 (2014) 992–1005.
[8] J. Pang, R.G. Mendes, A. Bachmatiuk, L. Zhao, H.Q. Ta, T. Gemming, H. Liu, Z. Liu, M.H. Rummeli, Applications of 2D MXenes in energy conversion and storage systems, Chem. Soc. Rev. 48 (1) (2019) 72–133.
[9] M. Naguib, M. Kurtoglu, V. Presser, J. Lu, J. Niu, M. Heon, L. Hultman, Y. Gogotsi, M.W. Barsoum, Two-Dimensional Nanocrystals Produced by Exfoliation of Ti_3AlC_2, Adv. Mater. 23 (37) (2011) 4248–4253.
[10] M.W. Barsoum, M.A.X. Phases, Properties of Machinable Carbides and Nitrides, Wiley VCH GmbH & Co., Weinheim, 2013.
[11] M. Alhabeb, K. Maleski, B. Anasori, P. Lelyukh, L. Clark, S. Sin, Y. Gogotsi, Guidelines for Synthesis and Processing of Two-Dimensional Titanium Carbide ($Ti_3C_2T_x$ MXene), Chem. Mater. 29 (18) (2017) 7633–7644.
[12] L. Verger, C. Xu, V. Natu, H.-M. Cheng, W. Ren, M.W. Barsoum, Overview of the Synthesis of MXenes and Other Ultrathin 2D Transition Metal Carbides and Nitrides, Curr. Opin, Solid State Mater. Sci. 23 (3) (2019) 149–163.
[13] L.-Å. Näslund, P.O.Å. Persson, J. Rosen, X-ray Photoelectron Spectroscopy of Ti_3AlC_2, $Ti_3C_2T_z$, and TiC Provides Evidence for the Electrostatic Interaction between Laminated Layers in MAX-Phase Materials, J. Phys. Chem. C 124 (50) (2020) 27732–27742.
[14] M. Khazaei, A. Mishra, N.S. Venkataramanan, A.K. Singh, S. Yunoki, Recent Advances in MXenes: From Fundamentals to Applications, Curr. Opin. Solid State Mater. Sci. 23 (3) (2019) 164–178.
[15] Z. Xia, Q. Huang, S. Guo, Recent Progress on Synthesis, Structure and Electrocatalytic Applications of MXenes, FlatChem 17 (2019), 100129.
[16] P.O.Å. Persson, J. Rosen, Current State of the Art on Tailoring the MXene Composition, Structure, and Surface Chemistry, Curr. Opin. Solid State Mater. Sci. 23 (2019), 100774.
[17] V. Natu, M. Benchakar, C. Canaff, A. Habrioux, S. Célérier, M.W. Barsoum, A critical analysis of the X-ray photoelectron spectra of $Ti_3C_2T_z$ MXenes, Matter 4 (4) (2021) 1224–1251.
[18] J. Halim, K.M. Cook, M. Naguib, P. Eklund, Y. Gogotsi, J. Rosen, M.W. Barsoum, X-ray photoelectron spectroscopy of select multi-layered transition metal carbides (MXenes), Appl. Surf. Sci. 362 (2016) 406–417.
[19] I. Persson, L.-Å. Näslund, J. Halim, M.W. Barsoum, V. Darakchieva, J. Palisaitis, J. Rosen, P.O.Å. Persson, On the organization and thermal behavior of functional groups on Ti_3C_2 MXene surfaces in vacuum, 2D Mater. 5 (2018), 015002.
[20] T. Schultz, N.C. Frey, K. Hantanasirisakul, S. Park, S.J. May, V.B. Shenoy, Y. Gogotsi, N. Koch, Surface Termination Dependent Work Function and Electronic Properties of $Ti_3C_2T_x$ MXene, Chem. Mater. 31 (2019) 6590–6597.
[21] M. Benchakar, L. Loupias, C. Garnero, T. Bilyk, C. Morais, C. Canaff, N. Guignard, S. Morisset, H. Pazniak, S. Hurand, P. Chartier, J. Pacaud, V. Mauchamp, M. W. Barsoum, A. Habrioux, S. Célérier, One MAX Phase, Different MXenes: A Guideline to Understand the Crucial Role of Etching Conditions on $Ti_3C_2T_x$ Surface Chemistry, Appl. Surf. Sci. 530 (2020), 147209.
[22] D.R. Baer, G.E. McGuire, K. Artyushkova, C.D. Easton, M.H. Engelhard, A.G. J. Shard, Introduction to Topical Collection: Reproducibility Challenges and Solutions with a Focus on Guides to XPS Analysis, J. Vac. Sci. Technol. A 39 (2021), 021601.
[23] G.H. Major, N. Farley, P.M.A. Sherwood, M.R. Linford, J. Terry, V. Fernandez, K. Artyushkova, Practical Guide for Curve Fitting in X-ray Photoelectron Spectroscopy, J. Vac. Sci. Technol. A 38 (2020), 061203.
[24] M. Magnuson, L.-Å. Näslund, Local chemical bonding and structural properties in Ti_3AlC_2 MAX phase and $Ti_3C_2T_x$ MXene probed by Ti 1s X-ray absorption spectroscopy, Phys. Rev. Research 2 (2020), 033516.
[25] L.-Å. Näslund, M.-H. Mikkelä, E. Kokkonen, M. Magnuson, Chemical Bonding of Termination Species in 2D Carbides Investigated through Valence Band UPS/XPS of Ti_3C_2Tx MXene, 2D Mater. 8 (2021), 045026.
[26] WaveMetrics, Igor Pro version 6.22A, https://www.wavemetrics.com/, accessed: February, 2011.
[27] S. Wendt, R. Schaub, J. Matthiesen, E.K. Vestergaard, E. Wahlström, M. D. Rasmussen, P. Thostrup, L.M. Molina, E. Lægsgaard, I. Stensgaard, B. Hammer, F. Besenbacher, Oxygen vacancies on TiO_2(110) and their interaction with H_2O and O_2: a combined high-resolution STM and DFT study, Surf. Sci. 598 (2005) 226–245.
[28] S. Wendt, J. Matthiesen, R. Schaub, E.K. Vestergaard, E. Lægsgaard, F. Besenbacher, B. Hammer, Formation and Splitting of Paired Hydroxyl Groups on Reduced TiO_2(110), Phys. Rev. Lett. 96 (2006), 066107.
[29] J.V. Lauritsen, A.S. Foster, G.H. Olesen, M.C. Christensen, A. Kühnle, S. Helveg, J. R. Rostrup-Nielsen, B.S. Clausen, M. Reichling, F. Besenbacher, Chemical identification of point defects and adsorbates on a metal oxide surface by atomic force microscopy, Nanotechnology 17 (14) (2006) 3436–3441.
[30] O. Bikondoa, C.L. Pang, R. Ithnin, C.A. Muryn, H. Onishi, G. Thornton, Direct visualization of defect-mediated dissociation of water on TiO_2(110), Nat. Mater. 5 (3) (2006) 189–192.
[31] C.L. Pang, A. Sasahara, H. Onishi, Q. Chen, G. Thornton, Noncontact atomic force microscopy imaging of water dissociation products on TiO_2(110), Phys. Rev. B 74 (2006), 073411.
[32] Z. Zhang, O. Bondarchuk, B.D. Kay, J.M. White, Z. Dohnálek, Imaging Water Dissociation on TiO_2(110): Evidence for Inequivalent Geminate OH Groups, J. Phys. Chem. B 110 (2006) 21840–21845.
[33] S. Yamamoto, H. Bluhm, K. Andersson, G. Ketteler, H. Ogasawara, M. Salmeron, A. Nilsson, In situ x-ray photoelectron spectroscopy studies of water on metals and oxides at ambient conditions, J. Phys.: Condens. Matter 20 (2008) 184025.
[34] A. Einstein, Concerning an Heuristic Point of View Toward the Emission and Transformation of Light, Ann. Physik 17 (1905) 132–148.
[35] S. Hüfner, Photoelectron Spectroscopy: Principles and Applications, third ed., Springer-Verlag, Berlin, 2010.
[36] G. Greczynski, L. Hultman, C1s Peak of Adventitious Carbon Aligns to the Vacuum Level: Dire Consequences for Material's Bonding Assignment by Photoelectron Spectroscopy, ChemPhysChem 18 (2017) 1507–1512.
[37] S. Doniach, M. Sunjic, Many-electron singularity in X-ray photoemission and X-ray line spectra from metals, J. Phys. C: Solid State Phys. 3 (2) (1970) 285–291.
[38] D.R. Baer, K. Artyushkova, H. Cohen, C.D. Easton, M. Engelhard, T.R. Gengenbach, G. Greczynski, P. Mack, D.J. Morgan, A. Roberts, X.P.S. Guide, Charge Neutralization and Binding Energy Referencing for Insulating Samples, J. Vac. Sci. Technol. A 38 (2020), 031204.
[39] J. Stöhr, NEXAFS spectroscopy, Springer-Verlag, New York, 1992.
[40] N. Mårtensson, R. Nyholm, Electron Spectroscopic Determinations of M and N Core-Hole Lifetimes for the Elements Nb-Te (Z= 41–52), Phys. Rev. B 24 (1981) 7121–7134.
[41] H. Siegbahn, L. Asplund, P. Kelfve, The Auger electron spectrum of water vapour, Chem. Phys. Lett. 35 (3) (1975) 330–335.
[42] L.-Å. Näslund, Reaction kinetics for the oxygen hydrogenation process on Pt(111) derived from temperature-programmed XPS, Surf. Sci. 618 (2013) 42–48.
[43] T. Ichinose, H. Monjushiro, H. Watarai, Charge-up Phenomena of Insulated Metals in X-ray Photoelectron Spectroscopy, Anal. Sci. 12 (1) (1996) 43–47.
[44] D.R. Baer, A.G. Shard, Role of Consistent Terminology in XPS Reproducibility, J. Vac. Sci. Technol. A 38 (2020), 031203.
[45] F. Werfel, O. Brümmer, Corundum Structure Oxides Studied by XPS, Phys. Scr. 28 (1) (1983) 92–96.
[46] M.D. Tucker, Z. Czigány, E. Broitman, L.-Å. Näslund, L. Hultman, J. Rosen, Filtered pulsed cathodic arc deposition of fullerene-like carbon and carbon nitride films, J. Appl. Phys. 115 (2014), 144312.
[47] D.R. Cousens, B.J. Wood, J.Q. Wang, A. Atrens, Implications of specimen preparation and of surface contamination for the measurement of the grain boundary carbon concentration of steels using x-ray microanalysis in an UHV FESTEM, Surf. Interface Anal. 29 (1) (2000) 23–32.
[48] M.H. Engelhard, D.R. Baer, A. Herrera-Gomez, P.M.A. Sherwood, Introductory guide to backgrounds in XPS spectra and their impact on determining peak intensities, J. Vac. Sci. Technol. A 38 (2020), 063203.
[49] S. Tougaard, Practical algorithm for background subtraction, Surf. Sci. 216 (3) (1989) 343–360.
[50] A. Herrera-Gomez, D. Cabrera-German, A.D. Dutoi, M. Vazquez-Lepe, S. Aguirre-Tostado, P. Pianetta, D. Nordlund, O. Cortazar-Martinez, A. Torres-Ochoa, O. Ceballos-Sanchez, L. Gomez-Muñoz, Intensity modulation of the Shirley background of the Cr 3p spectra with photon energies around the Cr 2p edge, Surf Interface Anal. 50 (2) (2018) 246–252.
[51] L.H. Karlsson, J. Birch, J. Halim, M.W. Barsoum, P.O.Å. Persson, Atomically Resolved Structural and Chemical Investigation of Single MXene Sheets, Nano Lett. 15 (8) (2015) 4955–4960.
[52] M.A. Hope, A.C. Forse, K.J. Griffith, M.R. Lukatskaya, M. Ghidiu, Y. Gogotsi, C. P. Grey, NMR reveals the surface functionalisation of Ti_3C_2 MXene, Phys. Chem. Chem. Phys. 18 (7) (2016) 5099–5102.